NeuroImage 189 (2019) 180–191

Contents lists available at ScienceDirect

NeuroImage

journal homepage: www.elsevier.com/locate/neuroimage

Amyloid-beta induced retrograde axonal degeneration in a mouse tauopathy model

Christopher Nishioka [a,b], Hsiao-Fang Liang [a], Barsam Barsamian [a,b], Shu-Wei Sun [a,b,c,*]

[a] Basic Sciences, School of Medicine, Loma Linda University, CA, USA
[b] Neuroscience Graduate Program, University of California, Riverside, USA
[c] Pharmaceutical Science, School of Pharmacy, Loma Linda University, CA, USA

ARTICLE INFO

Keywords:
Amyloid beta
p301L tau
Diffusion tensor imaging
Retrograde degeneration
Retinal ganglion cell
EpoD

ABSTRACT

White matter abnormalities, revealed by Diffusion Tensor Imaging (DTI), are observed in patients with Alzheimer's Disease (AD), representing neural network deficits that underlie gradual cognitive decline in patients. However, how DTI changes related to the development of Amyloid beta (Aβ) and tau pathology, two key hallmarks of AD, remain elusive. We hypothesized that tauopathy induced by Aβ could initiate an axonal degeneration, leading to DTI-detectable white matter abnormalities. We utilized the visual system of the transgenic p301L tau mice as a model system. Aβ was injected in Lateral Geniculate Nucleus (LGN), where the Retinal Ganglion Cell (RGC) axons terminate. Longitudinal DTI was conducted to detect changes in the optic tract (OT) and optic nerve (ON), containing the distal and proximal segments of RGC axons, respectively. Our results showed DTI changes in OT (significant 13.2% reduction in axial diffusion, AxD vs. vehicle controls) followed by significant alterations in ON AxD and fractional anisotropy, FA. Histology data revealed loss of synapses, RGC axons and cell bodies resulting from the Aβ injection. We further tested whether microtubule-stabilizing compound Epothilone D (EpoD) could ameliorate the damage. EpoD co-treatment with Aβ was sufficient to prevent Aβ-induced axon and cell loss. Using an acute injection paradigm, our data suggest that EpoD may mediate its protective effect by blocking localized, acute Aβ-induced tau phosphorylation. This study demonstrates white matter disruption resulting from localized Aβ, the importance of tau pathology induction to changes in white matter connectivity, and the use of EpoD as a potential therapeutic avenue to prevent the axon loss in AD.

1. Introduction

Alzheimer's Disease (AD) is a devastating, age-dependent neurodegenerative disease characterized by progressive declines in learning, memory, and executive functions of patients. These cognitive deficits likely arise in part due to the dysfunction within brain networks, including white matter (WM) tracts. Loss of WM microstructural integrity, detected by Diffusion Tensor Imaging (DTI), has been reported in patients with mild cognitive impairment (MCI) and AD (Yoshita et al., 2006; McAleese et al., 2015; Nir et al., 2013; Nishioka et al., 2015). The magnitude of DTI WM alterations correlates with cognitive performance, making WM damage a likely contributor to the symptoms experienced by patients and key to understanding AD pathophysiology (Nir et al., 2013).

Tracts damaged in AD typically include those which contain axons projecting to and from the medial temporal lobe (MTL) such as the parahippocampal cingulum, fornix and uncinate faciculus (Nir et al., 2013; Sexton et al., 2011; Liu et al., 2011). As tau pathology manifests initially in MTL structures of AD brains, it has been speculated that DTI-detected WM changes may be related to tau pathology (Kantarci et al., 2017). Tau, normally an axonal microtubule-binding protein, becomes abnormally hyperphosphorylated, folded, and prone to aggregation during AD. Hyperphosphorylated tau becomes dissociated from microtubules, leading to impaired axonal transport and dystrophic axons (Masliah et al., 1993; Mitew et al., 2010; Benes et al., 1991; De Vos et al., 2008). A class of dystrophic axons, neuropil threads, are filled with phospho-tau aggregates and formed early in the disease (Vana et al., 2011; Ghoshal et al., 2002). Resulting aggregates are associated with local induction of caspase-6, which has been implicated in precipitating axonal degeneration (Guo et al., 2004; Nikolaev et al., 2009; Uribe et al., 2012). These findings may implicate tau pathology spreading through axons as a primary event leading to progressive degeneration in AD.

Although the full scope of interactions between Aβ and tau pathology

* Corresponding author. Basic Sciences, School of Medicine, Loma Linda University, 11175 Campus Street, CSPC1023, Loma Linda, CA, 92354, USA.
E-mail address: rsun@llu.edu (S.-W. Sun).

https://doi.org/10.1016/j.neuroimage.2019.01.007
Received 19 July 2018; Received in revised form 27 December 2018; Accepted 4 January 2019
Available online 7 January 2019

remains a topic of intense research, studies suggest that intracellular tau pathology can be exacerbated by the presence of extracellular Aβ (Pooler et al., 2015; Ahmed et al., 2014; Bennett et al., 2017; Selenica et al., 2013). Furthermore, Aβ-induced tau pathology may spread through axons in a retrograde manner (Pooler et al., 2015; Bolmont et al., 2007; Gotz et al., 2001). As shown in a landmark study by Gotz et al., extracellular accumulations of Aβ can stimulate tau phosphorylation and aggregation in neurons with axons projecting into the injection site in mice expressing the mutant FTDP-17 (p301L) form of human tau, but not wild type mice (Bennett et al., 2017; Selenica et al., 2013; Gotz et al., 2001). P301L tau provides a tool for research to study tauopathy. Mice expressing the mutant variant exhibit well characterized age-dependant increases in neuronal tau pathology within cell bodies, dendrites and axons mimicking pathology observed in AD (Lewis et al., 2000).

To explore the pathological mechanisms leading to DTI-detectable WM alterations, we used an animal model to test whether distal injection of Aβ could induce tau-associated white matter damage detectable *in vivo* with DTI. We focused our investigation on the mouse visual system, which has well characterized neuronal identity and architecture and exhibits tau pathology in several cell types, including retinal ganglion cells (RGCs) (Ho et al., 2015). Mouse RGCs, whose cell bodies are in the retina, project axons into the brain through the optic nerve (ON) and optic tract (OT), before terminating in the lateral geniculate nucleus (LGN) (Sun et al., 2017). We examined changes in the visual system after Aβ injection into the left LGN using a combination of DTI, Optical Coherence Tomography (OCT), and end-stage histology. As mice have primarily monocular vision, with >95% of RGCs projecting into the contralateral side of the brain, the unaffected side of the visual system can serve as an internal control (Coleman et al., 2009; Drager and Olsen, 1980). Assuming axonal degeneration may be related to microtubule destabilization induced by tau pathology, microtubule-stabilizing drug Epothilone D (EpoD) intervention was tested to rescue the damage. The goal of this study is to yield important information about the process leading to axon loss during AD, link clinical imaging findings to tissue-level histology data, and provide potential therapeutic approaches for AD.

2. Materials and methods

All experimental procedures were in accordance with National Institutes of Health guidelines for the use of animals in research and were approved by the Institutional Animal Care and Use Committee of Loma Linda University.

2.1. Injection procedure

Human $A\beta_{1\text{-}42}$ (A9810, Sigma Aldrich, USA) was prepared using a modified version of a previously described protocol (Zago et al., 2012). Briefly, 1,1,1,3,3,3-hexafluoro-2-propanol (HFIP, Sigma) films from $A\beta_{1\text{-}42}$ peptide were dissolved in saline to a final concentration of 10 nmol/3 μL. Preparations were then incubated with shaking for 72 h at 37 °C. Mice were anesthetized by 1.5% isoflurane/oxygen using an isoflurane vaporizer (VetEquip, Pleasanton, CA). Body temperature was maintained using an electric heating pad during the procedure. Mice were placed in a stereotactic apparatus for injection guidance. Mouse heads were shaved and skin was cleaned with Povidine (Rugby Laboratories). After craniotomy, Aβ was injected slowly into the left LGN (coordinates: 2.46 mm posterior from Bregma, lateral 2.2 mm, 2.5 mm from cortical surface) using a 5-μl Hamilton syringe with an injection speed of 0.3 μl/min. The needle was kept in the injection site for an additional 10 min, then withdrawn 0.5 mm every 5 min until complete removal from the brain. The incision was then sutured and the animals were left to recover on an electric heating pad.

2.2. Longitudinal DTI/OCT examination

Mixed, littermate cohorts (50:50 M:F) of 10 month JNPL3 p301L tau mice were used for this experiment. Mice were injected with either 10 nmol Aβ (N = 8) or a vehicle saline solution (N = 8). Eight untreated mice were reserved as controls. Mice were scanned using MRI after 1 (n = 8 Aβ injected, n = 3 vehicle control), 4 (n = 8 Aβ, n = 5 vehicle) and 8 (n = 8 Aβ, n = 7 vehicle, n = 8 untreated control) weeks. We were limited by scanner availability thus not all mice were scanned at the earlier time points. Based on previous findings and preliminary data, we did not expect to see any significant asymmetry in DTI measures at any timepoints in untreated mice (Sun et al., 2015). To maximize scanner availability for treated groups, we opted to only scan at one timepoint of the untreated control group. OCT scans were collected from all mice in parallel at baseline (before injection) and again after 1, 4 and 8 weeks. Mice were sacrificed for histology immediately after final OCT and DTI examinations after 8 weeks.

Our lab previously has explored the degeneration induced by an Aβ injection in LGN of wild type mice, and we did not find axonal damage in optic tract or optic nerves (Sun et al., 2015). We hypothesized that misfolding-prone tau (p301L) might be required to interact with Aβ to induce neuronal axon loss, potentially through its prion-like seeding of the aggregated, hyperphosphorylated form. Appearance of tau aggregates in the brains of JNPL3 tau mice begins around 6 months in regions including the amygdala, midbrain and pons (Lewis et al., 2000). However, we only found robust exhibition of pathological tau deposition in the visual system later at 10 months of age. Thus, p301L mice at 10 months old were chosen to test whether Aβ could cause retrograde degeneration.

2.3. Epothilone D dosing experiment

Seven, 10 month old p301L mice were dosed with EpoD for eight weeks following Aβ injection. EpoD was purchased from Abcam (ab143615). EpoD dosed mice were given weekly intraperitoneal injections of Epod at 1 mg/kg dissolved in DMSO, starting one week prior to initial Aβ injection. In a previous study, prophylactic dosing with EpoD was sufficient to ameliorate axonal dystrophy (Brunden et al., 2010). In an effort to preempt early toxicity arising from Aβ-tau interactions, we began dosing one week prior to initial Aβ injections. Previous pharmacokinetic modeling experiments suggest that EpoD has a residence time in the brain >10 days after a single dose at 3 mg/kg (Brunden et al., 2010). The dose for this experiment was chosen based upon previous work by Brunden et al. and Zhang et al. in which EpoD at 1 mg/kg was sufficient to reduce measures of tauopathy, neurodegeneration and axonal dystrophy in PS19 tau mice (Brunden et al., 2010; Zhang et al., 2012). Mice were examined using OCT at baseline, before Aβ-injection then 1, 4 and 8 weeks after Aβ injection. All mice were sacrificed after 8 weeks for histology.

2.4. Acute Aβ administration experiment

In order to examine the acute effects of Aβ and EpoD on phospho-tau (p-tau) pathology, twelve p301L mice underwent Aβ injection. Six mice were pre-dosed with EpoD one week before Aβ injection and again on the day of injection. In each cohort, N = 2 were 10 month old, and N = 4 were 3 months old. These ages were chosen to separately examine the effects of Aβ and EpoD on the induction of tau pathology in aged mice with preexisting tau pathology (10 months) and younger mice without, in order to isolate the effects on tauopathy. All mice were then sacrificed after 3 days to examine tissue for histology.

2.5. DTI acquisition

MRI acquisitions were collected using a Bruker 11.7T BioSpec small animal MRI instrument using a Stejskal-Tanner spin-echo diffusion-weighted sequence. A set of 31 contiguous (gap-free) coronal slices were acquired to cover the brain with slice thickness 0.5 mm; FOV of 1.5 × 1.5 cm and matrix 128 × 128 (zero filled to 256 × 256); voxel size

58.6 μm × 58.6 μm x 500 μm; repetition time 2.5s; echo time 29 ms; δ 3 ms; Δ20 ms (where δ and Δ represent durations of the diffusion gradient and time between diffusion gradients, respectively). The data was zero filled to provide an apparent increase in spatial resolution. Twenty-one diffusion-weighted images based on the Icosa21 Tensor Encoding Schemes were acquired with $b = 0.85$ ms/um^2 along with two non-diffusion weighted scans (Hasan and Narayana, 2003). Raw diffusion-weighted images were processed using FSL (http://fsl.fmrib.ox.ac.uk/fsl/fslwiki/FDT), including steps for skull stripping and eddy current/motion correction using BET and Eddy modules, respectively. Corrected image sets were then loaded into 3D Slicer, and DTI maps including fractional anisotropy (FA), trace of diffusion (TR), axial diffusion (AxD) and radial diffusion (RAD) were created.

2.6. DTI analysis

ROIs were defined manually in the LGN, OT and ON. ON and OT ROIs were manually defined by a blinded observer using the high FA/low RAD which provide contrast against neighboring CSF and grey matter (Examples shown in Supplemental Fig. 1). ON DTI measures were made in two serial sections. Individual slices contained central regions within each ON with 8–12 voxels. OT regions were selected in two serial sections, comprising 50–60 voxels. LGN regions were defined using a mouse brain atlas as a reference and were bounded by the hippocampus (superior boundary) and external medually lamina (lateral boundary, high FA) (Franklin and Paxinos, 1997). Changes in diffusion metrics were computed by calculating the diffusional asymmetry (injected side [left LGN, OT and right ON]/un-injected side). This allowed each mouse to serve as its own control to reduce the degree of variability between animals.

Derived from DTI, the FA, TR, AxD and RAD metrics are sensitive to different aspects of nerve fiber disruption. AxD represents water diffusion along the primary axis of nerve fibers. This index is known to be sensitive to acute axonal damage as accumulation of neurofilaments may hinder diffusion along the length of fibers. RAD represents water diffusion across nerve fibers. This index is sensitive to myelin loss as well as late stages of axonal damage where increases of extracellular space can lead to increases of radial diffusivity. FA estimates how asymmetric water diffusion is in one direction. It is a combined effect of axial and radial diffusivities and usually is sensitive to overall white matter disruption. TR is the summation of diffusion in all directions, which is a combined effect of axial and radial diffusivities (Soares et al., 2013).

2.7. OCT acquisition

OCT imaging was performed using a BioOptigen Envisu C-Class. Our imaging protocol collected data from a 1.6 × 1.6 mm region centered on the optic disc. The protocol used 1000A scans/B Scan, 100 B scans total. B scans 320 μm and 240 μm superior and inferior to the optic disc (N = 4 per eye) were selected for analysis. These regions were selected for their consistent layer thickness characteristics. Images were processed and analyzed using custom software created in Matlab (Natick, MA). Individual B scans were pre-processed by manually removing retinal segments containing blood vessels along the RNFL surface. A fitted quadratic curve was then used to adjust individual A-scan positions to straighten the retina. All scans were manually reviewed to assure the straightness of each B scan. With the resulting straightened B scan, all scans were averaged, and the profile of intensity variation across of retina was plotted. Measurement of Ganglion cell complex (GCC) layer thickness was made based upon the intensity differences between layers. The GCC, which is composed of the soma, dendrites and axons of RGCs was defined as the distance between the retinal nerve fiber layer (RNFL) peak intensity and the intermediate border between the inner plexiform layer (IPL) maxima and the underlying Inner nuclear layer (INL) minima.

3. Histology

Mice were anesthetized and perfused with 4 °C PBS, then 4% paraformaldehyde. After perfusion, tissues were immersed in decalcification buffer for one week. Tissues were then sliced into 3 mm-thick sections and processed for paraffin embedding. Resulting paraffin blocks were then sectioned at 5 μm for sections of ON, OT, Retina and LGN.

Tissue sections were immunostained for markers of healthy axons (phosphorylated neurofilament, SMI-31, 1:1000; Covance), myelin sheaths (MBP, 1:1000; Zymed Inc), Aβ (1:100; ThermoFisher), presynaptic terminals (Synapsin-1, 1:2000; Cell Signaling), and Phospho-tau (p-tau, AT8, 1:400; ThermoFisher). Briefly, sections were deparaffinized, permeabilized in 0.3% Triton X-100, boiled in citrate buffer pH6, blocked in 3% NGS then incubated overnight in 1° antibodies. Fluorescently labeled sections were then incubated in appropriate 2° antibodies for 1hr and mounted for imaging. Brightfield detection of 1° antibodies was carried out using the Universal Quick HRP Kit (Vector labs) and counterstained with hematoxylin. Slides were imaged using a Keyence microscope using identical acquisition settings. Stained sections were analyzed using ImageJ.

3.1. Immunohistochemistry analysis

Axon and myelin immunohistochemistry (SMI31/MBP) were quantified in the OT using tissue sections imaged at 10x, from ~Bregma −1.82. Images from the left and right OT were acquired, using identical acquisition settings, below the threshold for image saturation. ROIs were drawn around the entire OT and mean pixel brightness was measured. These measurements were used to compute intensity asymmetry between left and right OTs. In the ON, axon numbers and AT8+ axons were measured using coronal sections through each nerve. Stained ONs were imaged using a 40× objective, then analyzed using the threshold and analyze particles segmentation functions in ImageJ.

Three retinal sections from each eye within 200 μM of the optic disc were selected for fluroro-Nissl staining (NeuroTrace, ThermoFisher). After staining, sections were imaged at 20x using ImageJ. Images were acquired within the central 1 mm portion of each retina. RGC cell bodies were counted in the most superficial retinal layer and calculated as RGC density per unit μM.

General tau pathology levels in the brain were assessed in p301L mice by AT8 immunohistochemisty in the CA1 region of the hippocampus. An ROI 500 μM wide was placed in the most superior region of the CA1b, capturing the stratum oriens, pyramidale and radiatum layers. Percent area measurements were performed to determine the p-tau burden in each hippocampus. Tau pathology induction after acute Aβ injections was measured in the CA3 region of the hippocampus. This region facilitated straightforward identification of neuronal p-tau in the pyramidal layers, (500 μM span) in the most medial region of CA3 adjacent to the Dentate Gyrus.

3.2. Statistical analysis

All results are expressed as mean ± standard deviation (SD). Asymmetry ratios of DTI data, (e.g. injected side/uninjected side FA_i/FA_u from ON) and histology measures (e.g. $SMI31_i/SMI31_u$) were calculated for analysis. DTI data were analyzed using a linear mixed model approach to test for effects of timepoint (1, 4 or 8 weeks post injection) treatment (Aβ or vehicle) and timepoint × treatment interactions. To control false discovery rate, Benjamini-Hochberg procedure was applied with a false discovery rate of 0.1 (Benjamini and Hochberg, 1995, 2000). To evaluate treatment effects on DTI parameters between experimental and vehicle control groups, data were compared at each timepoint using Man-Whitney *U* test. Single group data were compared between timepoints using the Friedman test. Histology data was analyzed using a one-way ANOVA. Correction for multiple comparisons was applied using post-hoc Tukey's test after ANOVA and Dunn's test after the Freidman

test. Correlations between DTI metrics and histology measures of axon and myelin were performed using a Pearson's correlation coefficient. All *p* values below $p < 0.05$ were considered statistically significant. Analysis were performed in Prism Graphpad (La Jolla, CA) and SPSS (Chicago, IL).

4. Results

4.1. DTI and OCT alterations to the visual pathway after Aβ injection

Examination of the visual system allowed us to collect data from the LGN, OT and ON by DTI as well as the retinal structure by OCT (Fig. 1a and b). One week after injections, mice were imaged using DTI to confirm the injection location and determine if there were any early alterations to visual system microstructure. The injection needle trace was visible, confirming successful LGN targeting. In the Aβ-injected LGN, we found initial reduction in diffusion was transient and recovered to a normal level after 4 (asymmetry $= 1.03 \pm 0.055$, $p < 0.05$) and 8 weeks (asymmetry $= 1.07 \pm 0.053$, $p < 0.05$).

The DTI findings are shown in Figs. 2 and 3. Pseudocolored DTI images are shown from a single animal revealing the changes in FA, AxD and RAD in the OTs (Fig. 2) and ONs (Fig. 3) across the time-course after Aβ injection. After one week, the left and right OTs show high FA and AxD. After four weeks, reduction of FA and AxD selectively on the Aβ-injected side can be seen. At eight weeks, reduced FA can be seen on the injected side, relative to the uninjected side, without strong effects on AxD. Within the ON, after one and four week timepoints, diffusion metrics from the uninjected and injected sides are similar. After eight weeks, reductions in FA and AxD are apparent on the injected side, relative to the uninjected side.

Within the OT, linear mixed model analysis revealed an effect of Aβ treatment ($F = 8.742$, $p = 0.006$) upon FA asymmetry. Additionally, we found significant effects of Aβ treatment ($F = 7.344$, $p = 0.012$) as well as treatment × timepoint ($F = 4.289$, $p = 0.025$) on AxD asymmetry (Fig. 2). After four weeks, we observed statistically significant ($p < 0.05$) differences to DTI asymmetry in the OT between treatment groups; Aβ-treated mice showed significant reductions in AxD asymmetry (0.92 ± 0.059) vs. vehicle controls (1.06 ± 0.089) (Fig. 2). No significant changes between groups were observed after 8 weeks. Within the ON, we found no significant effects of treatment, timepoint or treatment × timepoint interactions. However, eight weeks after injection, we found significant ($p < 0.01$) reductions in FA asymmetry among Aβ-treated mice (0.85 ± 0.15) vs. vehicle controls (1.06 ± 0.13). Additionally, after eight weeks we observed significant reductions in AxD asymmetry among Aβ-treated mice (0.817 ± 0.098) vs. vehicle controls (1.01 ± 0.13, $p < 0.05$) and vs. group-matched one week data ($p < 0.001$, Fig. 3). Collectively, these results show the pattern of diffusion alterations that result from Aβ-injection into the LGN. Changes appeared first in the LGN and OT, then subsequently in the ON.

OCT measurements of GCC thickness asymmetry revealed no significant differences between groups (Vehicle, Aβ or Aβ/EpoD treated) at baseline or after 1, 4 or 8 weeks (Fig. 4).

4.2. Histological examinations of Aβ and vehicle treated mice

Eight weeks after Aβ injection, obvious reductions in Synapsin-1 (syn-1, a marker of presynaptic terminals labeling) were apparent in the

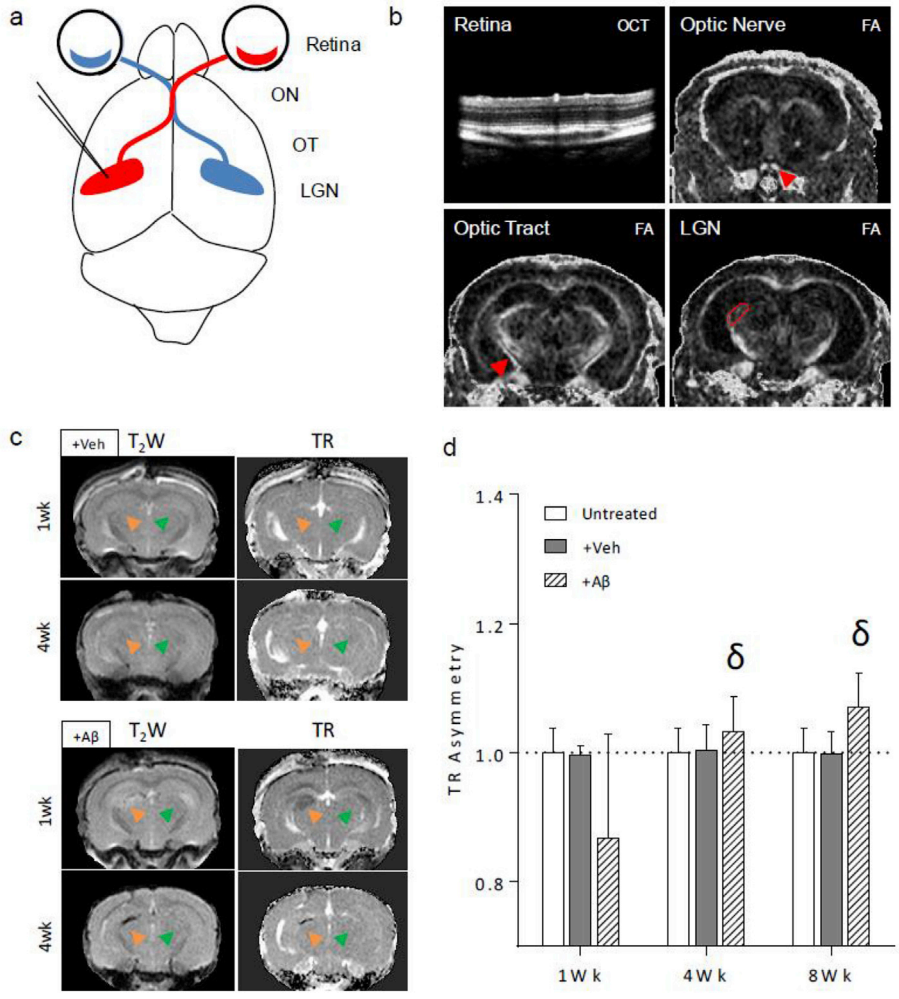

Fig. 1. (a) Diagram showing the mouse visual pathway and injected region. The pathway affected by the Aβ injection is shown in red. (b) In vivo images from OCT and FA DTI showing the examined structures including the retina, ON, OT and LGN. (c) T2-weighted and TR images from either Aβ or vehicle injected LGN-sections. Injected LGN is indicated by the orange arrow, with green indicating the untreated side. A transient reduction in LGN TR in the Aβ-injected side is visible at 1 wk. (d) Graph of TR asymmetry across the timecourse. "δ" Indicates data significantly different from group-matched 1 week data.

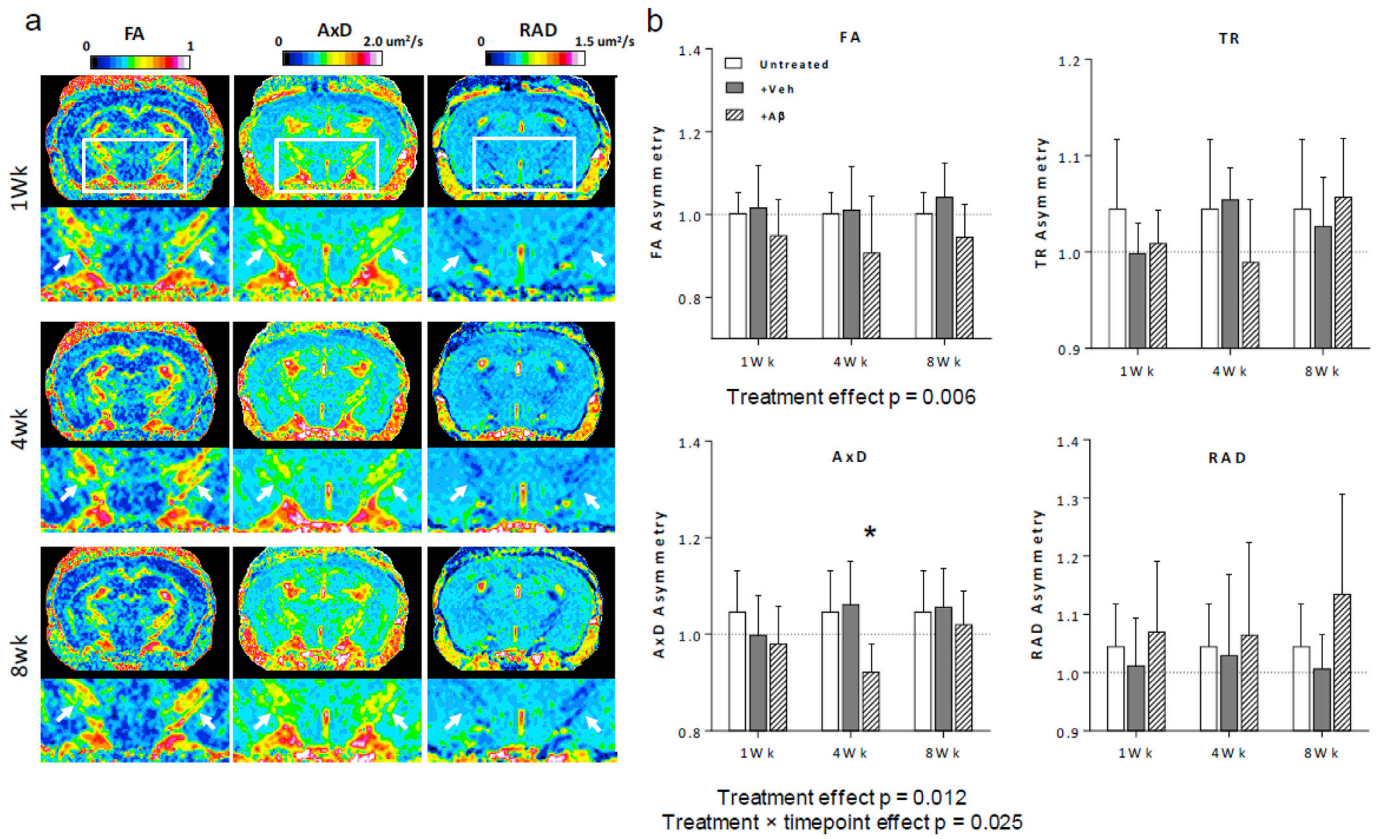

Fig. 2. DTI alterations within the Optic Tract. (a) Pseudocolored DTI images from a single animal showing the changes in FA, AxD and RAD across the time-course after Aβ injection. White arrows indicate the left (Aβ-injected) and right (uninjected) sides of the OT. After one week, the left and right OTs show high FA and AxD. After four weeks, FA and AxD are reduced selectively on the Aβ-injected side. At eight weeks, reduced FA can be seen on the injected side, relative to the uninjected side, without strong effects on AxD. (b) Quantification of DTI asymmetry in the OT. Significant reductions in AxD relative to vehicle controls are observed after 1 month. "*" Indicates significant differences from timepoint-matched vehicle controls.

injected LGN, relative to the contra-lateral side (Fig. 5). This reduction appeared to coincide with loss of tissue integrity in the LGN as well as the overlying CA3/Dentate Gyrus regions of the hippocampus to varying degrees among the Aβ-injected mice.

The ON and OT were examined using immunohistochemistry for markers of healthy axons (SMI31) and myelin (MBP, Fig. 6). Measurements of SMI31 intensity asymmetry (Aβ-affected side vs contralateral side) in OT revealed significant reductions in axon labeling among Aβ-injected mice (0.82 ± 0.087), relative to vehicle controls (0.98 ± 0.085, Fig. 6a). Within the ON, we found significant reductions in axon number asymmetry in Aβ-treated mice (asymmetry $= 0.71 \pm 0.22$), compared with vehicle-treated mice (0.98 ± 0.09, Fig. 6b). Measures of myelin intensity revealed no significant differences in the ON and OT between groups.

FluoroNissl-stained retinal sections were used for quantification of RGC cell bodies within the GCL sublayer (Fig. 6c). Density of cell bodies across the GCL was measured for each eye. Comparison of density asymmetry between groups revealed a significant ($p < 0.01$) reduction in cell bodies in the Aβ injected group (asymmetry $= 0.83 \pm 0.098$), compared to vehicle controls (1.04 ± 0.075).

Comparisons between DTI and histology datasets revealed significant correlations between ON FA ($r = 0.76$, $p = 0.001$), AxD ($r = 0.54$, $p = 0.038$) and RAD ($r = -0.671$, $p = 0.0062$) asymmetry measures and axon counts (Fig. 7). No significant relationships were observed between myelin staining and DTI measures.

4.3. Histological examination of tau pathology

Immunolabeling of tau phosphorylation was examined using the AT8 antibody (Fig. 8). We found a high degree of variability in the number and density of p-tau bearing axons between animals. This variability generally correlated with the degree of AT8+ staining observed within the GCC layers of the retina (Fig. 8b). However, we found no significant differences in p-tau axon density between left/right ONs in Aβ-injected and vehicle-treated mice (Fig. 8d). Additionally, we found no significant correlations between axon losses and density of AT8+ axons (Fig. 8e).

Severity of p-tau pathology was also quantified in the CA1 region of the hippocampus, as a general index of p-tau within the brain. The observed staining was concentrated within pyramidal neurons and their dendrites (Fig. 8c). As in the ON, we also observed large degrees of variance between different animals in the Aβ and vehicle-injected cohorts. We found a trend toward higher levels of tau pathology in the Aβ-treated cohort vs. vehicle control cohort, though no significant change was apparent.

4.4. Histological examination of Aβ/EpoD treated mice

In the LGN, EpoD dosing appeared to preserve Syn-1 labeling that was lost in Aβ-injected cohorts (Fig. 5). Similarly, we found EpoD dosing normalized SMI31 labeling asymmetry in the OT (Fig. 6a) and the ON (Fig. 6b) in the Aβ-injected mice. Additionally, EpoD-treated mice showed no significant RGC density asymmetry in the retina affected by Aβ (Fig. 6c). We found no differences in AT8+ axon numbers in the ON among these mice vs. vehicle controls (Fig. 8d). However, significant (>80%, $p < 0.01$) reductions in p-tau were apparent in the hippocampus, as compared with the Aβ-treated cohort (Fig. 8c,f).

4.5. Acute effects of Aβ and EpoD on tau pathology

To probe the acute effects of Aβ and EpoD in this experiment, we

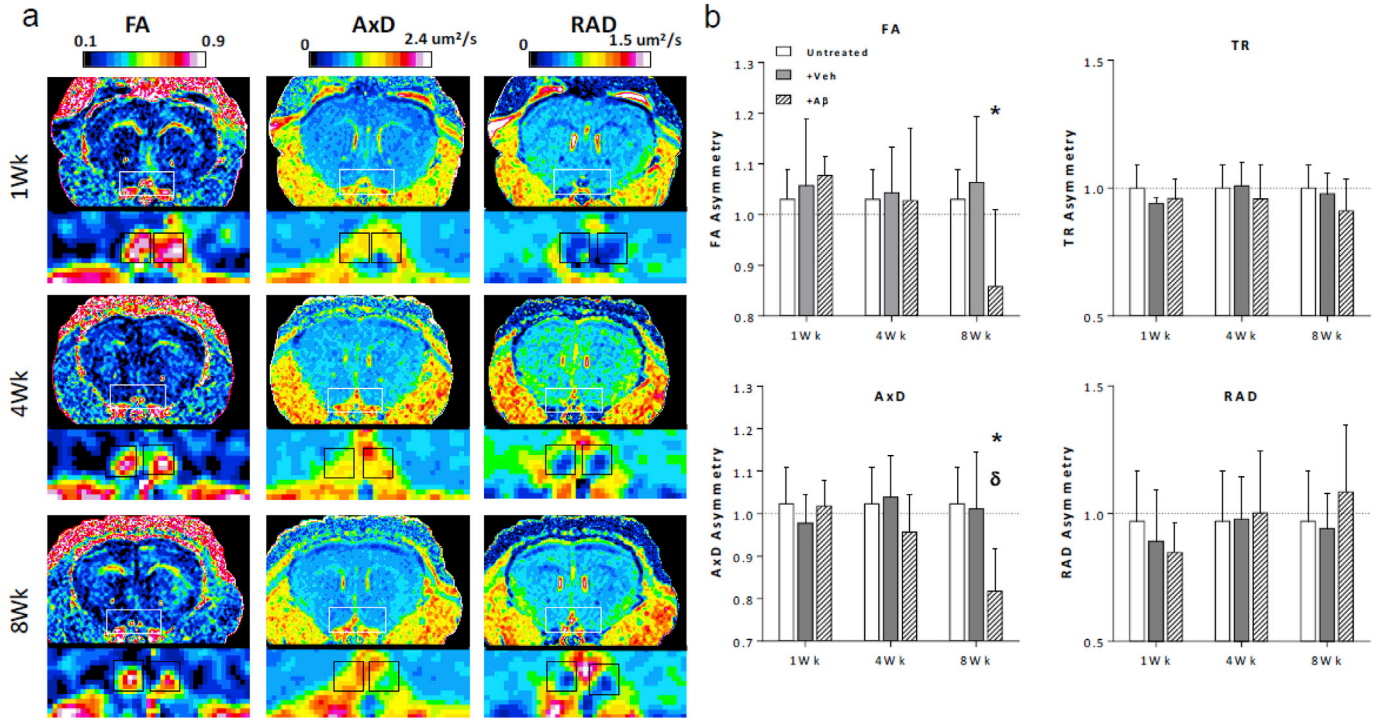

Fig. 3. DTI alterations within the ON (a) Pseudocolored DTI images from a single animal showing the changes in FA, AxD and RAD in the ON across the time-course after Aβ injection. Black boxes outline the left (uninjected) and right (injected) ONs. At one and four week timepoints, diffusion metrics from the uninjected and injected sides are similar. At eight weeks, reductions in FA and AxD are apparent on the injected side, relative to the uninjected side. (b) Quantification showing the changes in all DTI asymmetry metrics after 1, 4 and 8 weeks. "*" Indicates significantly difference from timepoint-matched vehicle controls, "δ" indicates significant difference from group-matched 1 week data.

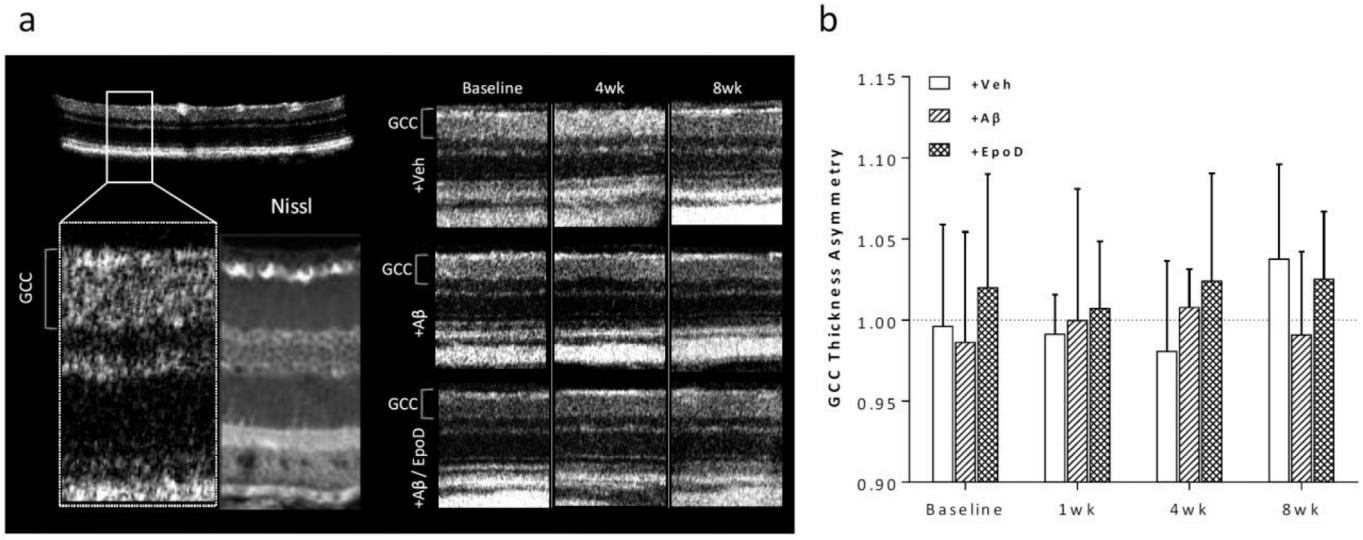

Fig. 4. OCT measurements of GCC layer thickness. (a) OCT B-scan and magnified region showing layer detail in comparison with Nissl-stained section. GCC layer (shown in green brackets) encompasses RNFL, GCL and IPL sublayers. Right, OCT B scans from the three experimental groups at baseline and after 4 and 8 weeks. (b) Graph showing GCC thickness asymmetry (between right and left retinas) at baseline (before injections) and again after 1, 4 and 8 weeks.

sacrificed twelve p301L mice 3 days after treatment (2 Aβ-injected, 2 Aβ/EpoD in 10 month old mice and 4 Aβ-injected, 4 Aβ/EpoD in 3 month old mice). In and around the injection site, we could see Aβ in the LGN and CA3 region of the Hippocampus (Fig. 9a). Surrounding the injection site, p-tau bearing neurons were evident. These increases were immediately apparent by comparisons to the contra-lateral Hippocampus/LGN (Fig. 9b). However, these increases in p-tau were not seen in mice pre-treated with both Aβ/EpoD. Additionally, no asymmetry in p-tau axon numbers was observed in ON sections. The experiment using 3-month p301L mice (4 Aβ-injected, 4 Aβ/EpoD) confirmed this result and ruled out the contribution of pre-existing pathology in aged mice. In this cohort, we found no existing p-tau pathology in ON axons from either cohort, but did find extensive p-tau pathology in Aβ-treated mice in both the hippocampus and LGN (Fig. 9c) exclusively on the injected side. Quantitative analysis was conducted on this cohort of mice (4 Aβ-injected, 4 Aβ/EpoD on 3-month p301L mice). EpoD significantly reduced p-

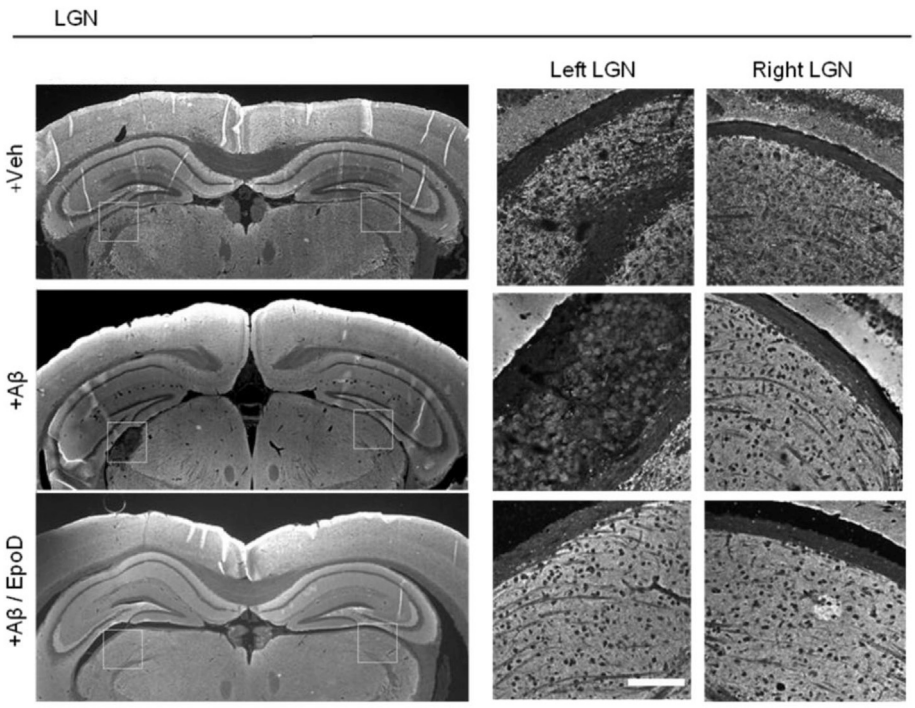

Fig. 5. Presyanptic terminal labeling in the LGN. Synapsin-1 immunohistochemistry of presynaptic terminal density across the brain. Selective loss of presynaptic terminals and tissue integrity were seen in the left LGN of Aβ-injected mice. Obvious terminal or tissue loss were not apparent in vehicle or EpoD-treated mice. Scale bar = 50 μm.

tau pathology, relative to mice receiving Aβ-treatment alone (Fig. 9d).

5. Discussion

In the present study, we tested whether retrograde axonal damage results from Aβ-induced tau pathology at sites distal from the cell body. Measuring visual system microstructural properties by DTI allowed us to connect noninvasive surrogate measures to discrete pathology, and link our data to clinical findings. Our data reveal that LGN Aβ injections lead to selective loss of WM integrity by DTI, which appears to correlate with axon loss. Longitudinal data suggest that alterations within the visual pathway manifest first in the LGN, OT and later in the ON, suggestive of a retrograde degeneration process. Additionally, our data suggest that the microtubule-stabilizing compound EpoD can prevent Aβ-induced tau phosphorylation and preempt downstream neurodegeneration.

Axonal damage and WM abnormalities in AD have been documented in numerous neuropathological studies (Shin et al., 1992; Umahara et al., 2002; Kowall and Kosik, 1987; Brun and Englund, 1986; Scheltens et al., 1995). The advent of DTI has facilitated the *in vivo* study of white matter microstructure alterations during the course of AD (Bosch et al., 2012). These alterations likely reflect the loss of connectivity within neural circuits, directly contributing to cognitive decline during AD. As such, research has been pursued to link DTI-detectable WM damage with specific AD pathologies, in particular using AD-related animal models. However, DTI studies examining AD-model mice have shown variable and at times contradictory results. APP-overexpressing models have shown reductions in white matter FA/RAD in several studies vs. non-transgenic controls (Sun et al., 2005; Song et al., 2004; Zerbi et al., 2013; Grandjean et al., 2016), and increases in these metrics in another (Shu et al., 2013). Tauopathy models have shown reductions in FA/RAD white matter in a pair of studies (Wells et al., 2015; Sahara et al., 2014), while the triple transgenic model (with combined APP/tau expression) does not reveal changes relative to controls (Kastyak-Ibrahim et al., 2013). This diversity of findings may reflect the heterogeneity of axon and neuron loss between AD models. Variable pathogenesis of axonal damage in AD, including the effects of tauopathy (microtubule disruption or impaired axonal transport) amyloid deposition and inflammation may lead to a diversity of DTI outcomes.

To examine the direct effects of Aβ on WM integrity, we previously conducted a study injecting a high-dose of Aβ into the LGN of wild-type C57Bl/6 mice. This approach allowed us to directly target axon terminals of RGCs without direct effects on RGC cell bodies. We observed weakened amplitude of the visual evoked potential (VEP), possibly by impairing synaptic function, but did not find DTI alterations in either the ON and OT of WT C57Bl/6 mice (Sun et al., 2015). Following from the work by Gotz et al., who demonstrated the ability of Aβ to induce p-tau accumulation in neurons of p301L tau mice (Gotz et al., 2001), we here revised our study and examined effects of our injection paradigm on tau mice. Previous studies have shown age-dependent development of tau aggregates in the brain of p301L mice, starting around 6 months. However, these early aggregates only present in select regions of brain, including the amygdala, hypothalamus, midbrain and pons (Lewis et al., 2000). Based on preliminary data, robust exhibition of pathological tau deposition does not occur in the visual system until more advanced ages. As a majority of p301L mice showed detectable levels of tau pathology in the visual system at 10 months, they were used to test whether Aβ in conjunction with tau pathology could induce retrograde axonal degeneration. We demonstrate that Aβ injections in p301L mice precipitate changes in DTI metrics as well as measureable axon loss. Collectively, our work demonstrates the critical role of pathological tau to enable Aβ-induced axonal damage and the temporospatial profile of axonal degeneration, which may propagate from the injection site toward cell bodies.

The relationship between DTI-detected WM changes and histologically detected axonal loss has been observed in several animal and human studies (Sun et al., 2017; Budde et al., 2009; Schmierer et al., 2007, 2008; Gouw et al., 2008). Similar to our findings, reductions in FA and increases in RAD were found to correlate with axon loss in abnormal WM in both MCI and AD patients (Sun et al., 2017; Budde et al., 2009; Schmierer et al., 2007, 2008; Gouw et al., 2008). DTI findings from this study do differ from human AD data with respect to the changes in AxD. In AD, AxD measures increase relative to controls, while we found

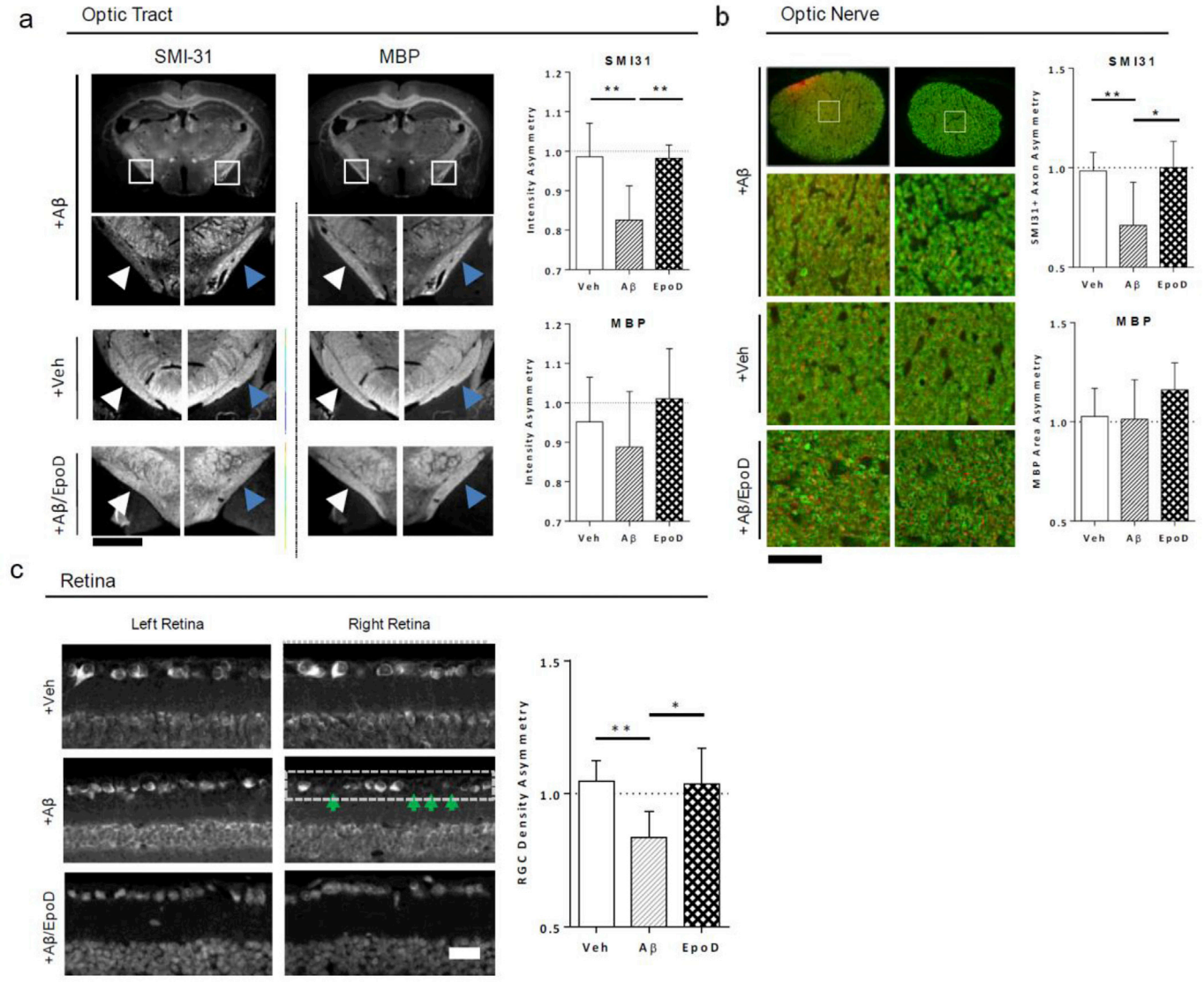

Fig. 6. IHC findings from the OT, ON and Retina (a) Staining for axons (SMI-31) and myelin (MBP) in the OT. Images show the differences in labeling intensity between left and right. Zoomed images show selective reductions in SMI-31 intensity in the left OT (white arrows), relative to the right OT in Aβ-injected mice (blue arrows). Black scale bar denotes 500 μm within the zoomed images. These changes are not apparent with MBP labeling. Right, quantification of SMI-31 and MBP OT intensity asymmetry. (b) Axon (red) and myelin (green) staining in the ON. Right, quantification of axon and myelin asymmetry in the ON. Selective reduction of axons but not myelin were seen in Aβ-treated mice. Black scale bar shows 25 μm (c) Retinal Nissl staining showing the Ganglion cell layer with selective loss of cell bodies (green arrows) in Aβ-injected mice. Right, quantification of RGC density asymmetry within the retinas of each experimental cohort. *, $p < 0.05$; **, $p < 0.01$.

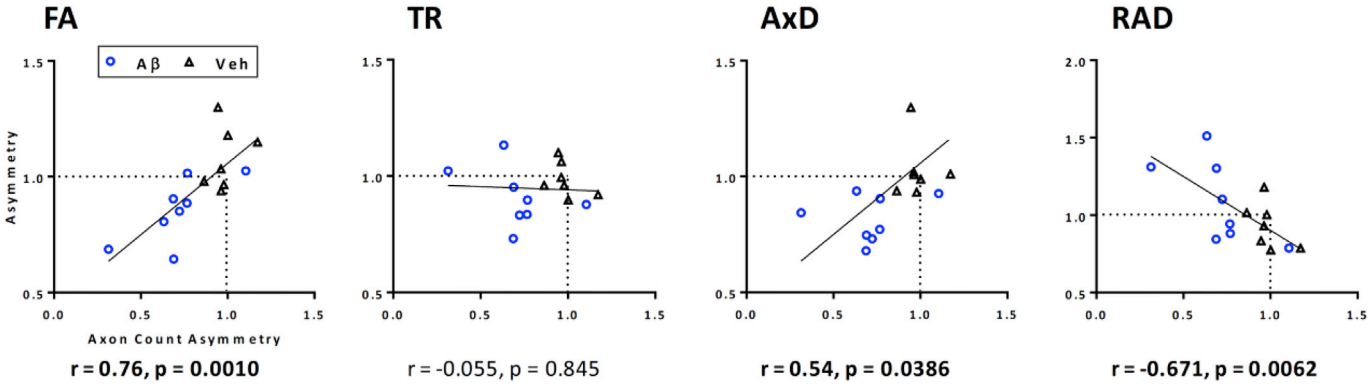

Fig. 7. Comparisons between DTI asymmetry and IHC-measured axon number asymmetry in the ON. Significant relationships were observed between axon number asymmetry and FA, AxD and TR asymmetry by DTI. No significant relationships between measures of myelination and DTI asymmetry were found.

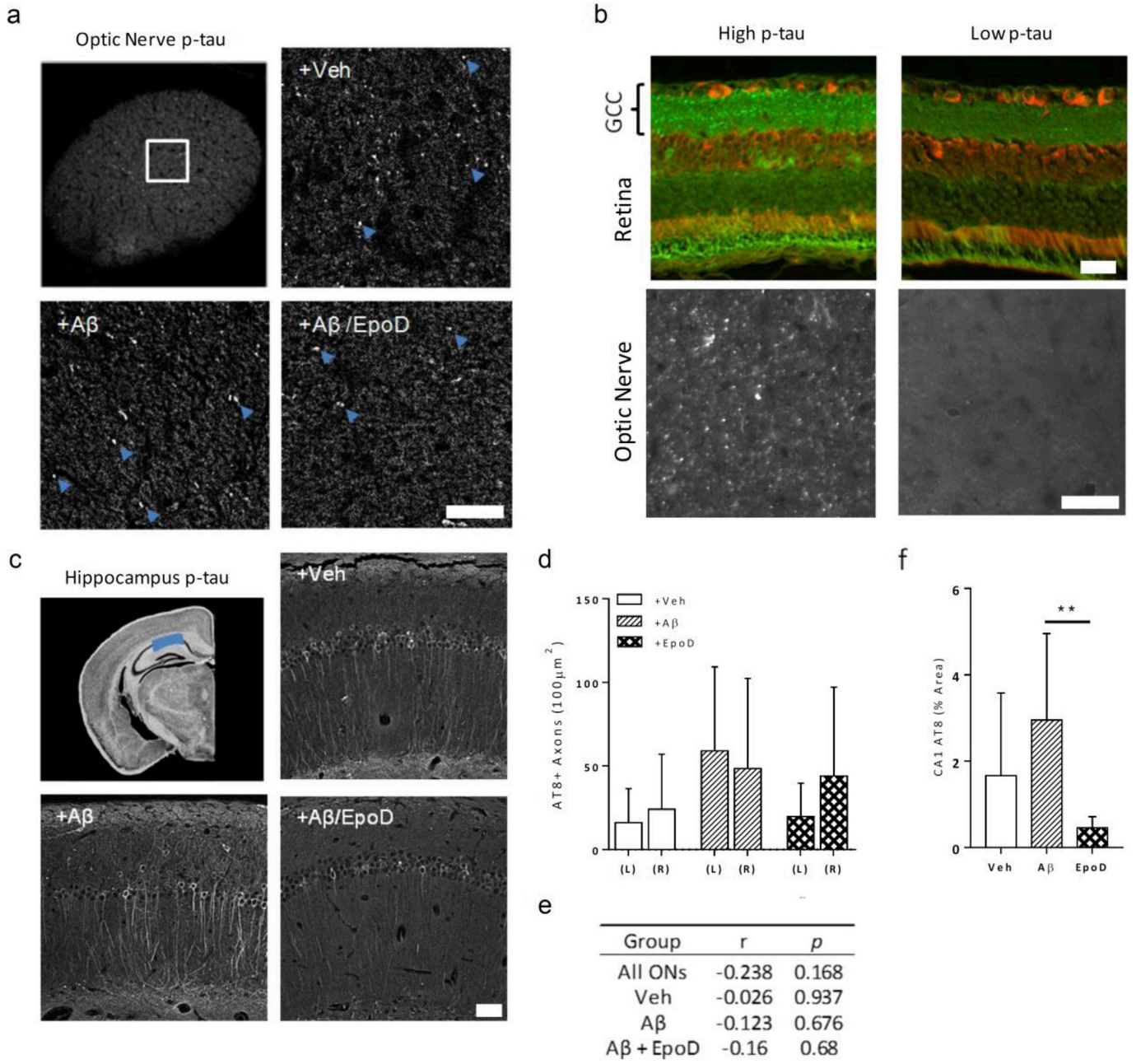

Group	r	p
All ONs	-0.238	0.168
Veh	-0.026	0.937
Aβ	-0.123	0.676
Aβ + EpoD	-0.16	0.68

Fig. 8. Phospho-tau staining in the ON and Hippocampus. (a) Phospho-tau (AT8) staining in the ON shows punctate axonal staining in the ON among all groups. White scale bar shows 25 μm. (b) Retinal sections labeled with p-tau (green) and colabeled with Fluoronissl (red). Representative sections showing high (left) and low (right) levels of p-tau labeling in retina, concentrated within the GCC. Lower sections show each retinas' respective ON section, labeled with AT8. Scale bars show 25 μm. (c) Top left image shows the ROI (blue) from the CA1 region of the hippocampus, where AT8+ staining was quantified, other images show representative levels of p-tau staining. Scale bar shows 100 μm. (d) Quantification of AT8+ axon density in left and right ONs among all groups (e) Correlations between ON axon density and AT8+ axon density. (f) AT8 staining revealed a significant reduction of phospho-tau staining in the hippocampus among Aβ/EpoD treated mice compared with Aβ treatment alone.**, $p < 0.01$.

reductions in measures of AxD (Bosch et al., 2012). This difference may be explained by microenvironment differences after acute vs. chronic axonal degeneration. AxD is thought to represent the diffusion along the lengths of fibers, whose reduction could be caused by cytoskeletal breakdown or focal 'beading' along axons (Budde and Frank, 2010). Reductions in AxD is observed in human WM during acute injury settings, as in optic neuritis (inflammation/neurodegeneration of the ON) (van der Walt et al., 2013). In mouse models, Reductions in AxD are also seen during acute axonal degeneration (Sun et al., 2017; Song et al., 2002). This reduction is transient, though and eventually increases relative to control subjects (van der Walt et al., 2013; Naismith et al., 2009). Our measurement of AxD may follow this pattern in the OT, which shows early (4 week) reduction, then later normalization by 8 weeks. Though these noninvasive measures give clues about pathological outcomes, they are only surrogate measures of white matter damage and/or axonal degeneration that need to be verified histologically.

The longitudinal DTI measurements enabled us to examine the temporospatial profile of axonal degeneration in our model system. We observed a 'dying-back' pattern emanating from the location of the Aβ injection, in which axons die-back from the synapse, leading to neuronal loss. These observations raise the prospect that degeneration could be initiated through synaptic or axonal mechanisms, independent of

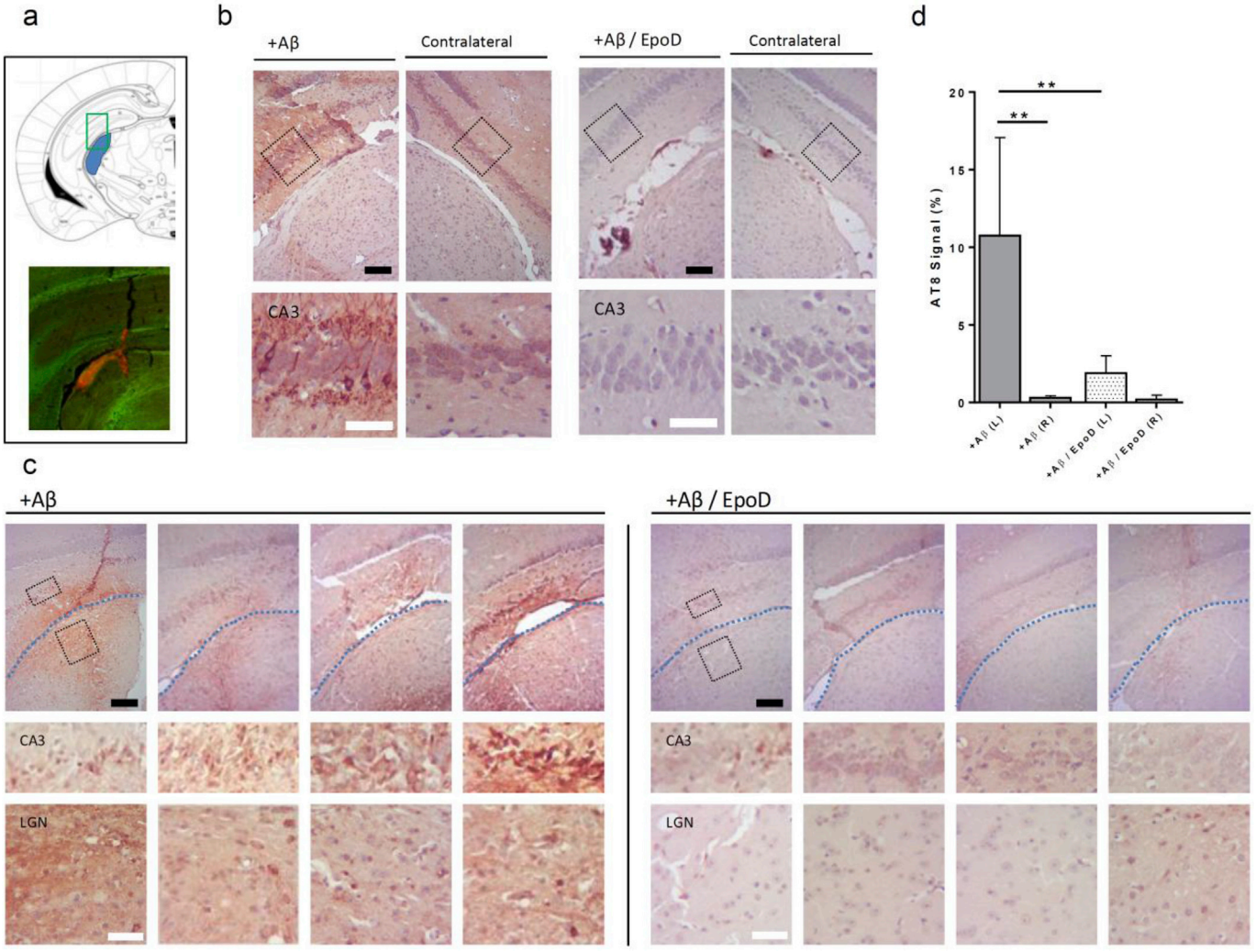

Fig. 9. Phospho-tau induction in the LGN and Hippocampus after acute Aβ injection. (a) Top, coronal atlas section shows the injection location. Bottom, zoomed-in region showing Aβ (red) within LGN and hippocampus 3 days after injection. (b) AT8+ p-tau staining in 10-month old p301L mice 3-days after injection. Abundant tau pathology is apparent in the injection region on the left side, but absent in the contralateral right LGN/hippocampus and in mice pre-treated with EpoD. (c) Young, 3 month old p301L mice show AT8+ p-tau pathology 3 days after Aβ injection in both the hippocampus and LGN on the left injected side. The blue line denotes the border between LGN and hippocampus. Mice pre-treated with EpoD before Aβ injection show greatly reduced tau pathology in hippocampus/LGN. Black scale bars show 100 μm, white bars show 50 μm. (d) Quantification of p-tau staining in the CA3 layer among 3 month old p301L mice. **, $p < 0.01$.

apoptosis, a mechanism which has been widely studied in other model systems, such as spinal cord injury and Multiple Sclerosis (Coleman and Freeman, 2010; Singh et al., 2017; Conforti et al., 2014). These findings suggest that axonal damage and dysfunction may be a key initial step in tau-mediated neurodegeneration. This idea is bolstered by evidence from AD tissue, suggestive of early axonal dysfunction preceding overt cell loss. This includes the presence of dystrophic axons, dsyfunctional axonal transport and cytoskeletal abnormalities early in the disease process (Kanaan et al., 2013; Kneynsberg et al., 2017). Notably, overexpression of nicotinamide mononucleotide adenylyl transferase 1 & 2 (NMNAT1 & 2), which delays the process of axonal disruption propagating from a transaction site, was found to be neuroprotective in tauopathy models (Ljungberg et al., 2012; Ali et al., 2012). Early interventions may delay the dying-back process and provide an opportunity to preserve neurons in patients with AD.

Our data suggest that microtubule stabilizers such as EpoD may have a therapeutic effect sufficient to reduce tau pathology as well as synapse, axon and cell losses induced by Aβ. These results are congruent with previous studies that have demonstrated the blood-brain-barrier permeability of the drug and its neuroprotective qualities in pure tauopathy models (Brunden et al., 2010; Zhang et al., 2012). Data from previous studies have found evidence that EpoD can promote axonal health by reducing axonal dystrophy, increasing ON microtubule density and normalizing fast axonal transport (Brunden et al., 2010; Zhang et al., 2012). Additionally, previous studies utilizing EpoD as well as microtubule-stabilizing peptide NAP have both shown ability to reduce p-tau pathology in AD model mice over several months of treatment (Zhang et al., 2012; Matsuoka et al., 2007, 2008). Our data recapitulate these findings, showing much lower levels of tau pathology among EpoD treated mice after two months of dosing. Furthermore, our data suggest that EpoD dosing prevents acute, local tau phosphorylation induced by Aβ that precedes later synapse, axon and cell loss.

While DTI measures on EpoD treated mice were originally included as part of our study design, unanticipated MRI service issues prevented the collection of these data. In a future study, we would like to directly assess the neuroprotective effects of EpoD on DTI measures and their correlation to tau pathology and tissue integrity by histology.

In addition to the use of 10 month old mice, we also explored using younger mice (3 months old) in order to rule out the contribution of pre-existing tau pathology on histological outcomes. As shown in Fig. 9, Aβ injection is able to induce local tauopathy even in mice without abundant pre-existing tau aggregates. These findings raise questions about whether

pre-existing tau aggregates are strictly necessary for Aβ to exert its neurotoxicity. Although tau aggregates are hallmarks of AD, several studies have suggested that oligomeric tau in soluble forms may be the most potent neurotoxic form (Wu et al., 2013; Iba et al., 2013, 2015; Stancu et al., 2015; Peeraer et al., 2015; Kopeikina et al., 2012). A future study in our model using DTI and OCT to examine changes in young mice (in comparison to the results of the present study) will extend our understanding of Aβ-tau interactions and their role in causing neurodegeneration during AD.

In summary, our data demonstrates that Aβ injection can induce retrograde axonal damage in p301L mice. This axonal damage can be detected by DTI, and the findings mirror several aspects of clinical data obtained from patients with AD. Our *in vivo* imaging approach paired with histology enabled us to detect the temporospatial profile of degeneration. Epothilone D administration is sufficient to prevent this damage, limiting the induction of p-tau pathology and preventing downstream degeneration in the OT, ON and RGCs.

Acknowledgements

This work was supported in part by the National Institutes of Health [grant numbers NS062830] and LLU School of Medicine through Grants to Promote Collaborative and Translational Research (GCAT). We also appreciated Dr. Iryna Ethell (University of California, Riverside) for insightful discussion about Aβ – tau interactions in the mechanisms of neurodegeneration in AD.

Appendix A. Supplementary data

Supplementary data to this article can be found online at https://doi.org/10.1016/j.neuroimage.2019.01.007.

References

Ahmed, Z., Cooper, J., Murray, T.K., et al., 2014. A novel in vivo model of tau propagation with rapid and progressive neurofibrillary tangle pathology: the pattern of spread is determined by connectivity, not proximity. Acta Neuropathol. 127, 667–683. https://doi.org/10.1007/s00401-014-1254-6, 2014/02/18.

Ali, Y.O., Ruan, K., Zhai, R.G., 2012. NMNAT suppresses tau-induced neurodegeneration by promoting clearance of hyperphosphorylated tau oligomers in a Drosophila model of tauopathy. Hum. Mol. Genet. 21, 237–250. https://doi.org/10.1093/hmg/ddr449.

Benes, F.M., Farol, P.A., Majocha, R.E., et al., 1991. Evidence for axonal loss in regions occupied by senile plaques in Alzheimer cortex. Neuroscience 42, 651–660, 1991/01/01. DOI: 0306-4522(91)90034-L [pii].

Benjamini, Y., Hochberg, Y., 1995. Controlling the false discovery rate - a practical and powerful approach to multiple testing. J. Roy. Stat. Soc. B 57, 289–300.

Benjamini, Y., Hochberg, Y., 2000. On the adaptive control of the false discovery rate in multiple testing with independent statistics. J. Educ. Behav. Stat. 25, 60–83.

Bennett, R.E., DeVos, S.L., Dujardin, S., et al., 2017. Enhanced tau aggregation in the presence of amyloid beta. Am. J. Pathol. 187, 1601–1612, 2017/05/14. DOI: S0002-9440(17)30080-9 [pii] 10.1016/j.ajpath.2017.03.011.

Bolmont, T., Clavaguera, F., Meyer-Luehmann, M., et al., 2007. Induction of tau pathology by intracerebral infusion of amyloid-beta -containing brain extract and by amyloid-beta deposition in APP x Tau transgenic mice. Am. J. Pathol. 171, 2012–2020, 2007/12/07. DOI: S0002-9440(10)62461-3 [pii] 10.2353/ajpath.2007.070403.

Bosch, B., Arenaza-Urquijo, E.M., Rami, L., et al., 2012. Multiple DTI index analysis in normal aging, amnestic MCI and AD. Relationship with neuropsychological performance. Neurobiol. Aging 33, 61–74. https://doi.org/10.1016/j.neurobiolaging.2010.02.004 S0197-4580(10)00082-5 [pii], 2010/04/08.

Brun, A., Englund, E., 1986. A white matter disorder in dementia of the Alzheimer type: a pathoanatomical study. Ann. Neurol. 19, 253–262. https://doi.org/10.1002/ana.410190306, 1986/03/01.

Brunden, K.R., Zhang, B., Carroll, J., et al., 2010. Epothilone D improves microtubule density, axonal integrity, and cognition in a transgenic mouse model of tauopathy. J. Neurosci. 30, 13861–13866. https://doi.org/10.1523/JNEUROSCI.3059-10.201030/41/13861 [pii], 2010/10/15.

Budde, M.D., Frank, J.A., 2010. Neurite beading is sufficient to decrease the apparent diffusion coefficient after ischemic stroke. Proc. Natl. Acad. Sci. U. S. A. 107, 14472–14477. https://doi.org/10.1073/pnas.1004841107 1004841107 [pii], 2010/07/28.

Budde, M.D., Xie, M., Cross, A.H., et al., 2009. Axial diffusivity is the primary correlate of axonal injury in the experimental autoimmune encephalomyelitis spinal cord: a quantitative pixelwise analysis. J. Neurosci. 29, 2805–2813. https://doi.org/10.1523/JNEUROSCI.4605-08.2009 29/9/2805 [pii], 2009/03/06.

Coleman, M.P., Freeman, M.R., 2010. Wallerian degeneration, wld(s), and nmnat. Annu. Rev. Neurosci. 33, 245–267. https://doi.org/10.1146/annurev-neuro-060909-153248, 2010/03/30.

Coleman, J.E., Law, K., Bear, M.F., 2009. Anatomical origins of ocular dominance in mouse primary visual cortex. Neuroscience 161, 561–571. https://doi.org/10.1016/j.neuroscience.2009.03.045, 2009/03/31.

Conforti, L., Gilley, J., Coleman, M.P., 2014. Wallerian degeneration: an emerging axon death pathway linking injury and disease. Nat. Rev. Neurosci. 15, 394–409. https://doi.org/10.1038/nrn3680 nrn3680 [pii], 2014/05/21.

De Vos, K.J., Grierson, A.J., Ackerley, S., et al., 2008. Role of axonal transport in neurodegenerative diseases. Annu. Rev. Neurosci. 31, 151–173. https://doi.org/10.1146/annurev.neuro.31.061307.090711, 2008/06/19.

Drager, U.C., Olsen, J.F., 1980. Origins of crossed and uncrossed retinal projections in pigmented and albino mice. J. Comp. Neurol. 191, 383–412. https://doi.org/10.1002/cne.901910306, 1980/06/01.

Franklin, K.B.J., Paxinos, G., 1997. The Mouse Brain in Stereotaxic Coordinates. Academic Press, San Diego, p. xxii, 186 p. of plates.

Ghoshal, N., Garcia-Sierra, F., Wuu, J., et al., 2002. Tau conformational changes correspond to impairments of episodic memory in mild cognitive impairment and Alzheimer's disease. Exp. Neurol. 177, 475–493, 2002/11/14. DOI: S0014488602980143 [pii].

Gotz, J., Chen, F., van Dorpe, J., et al., 2001. Formation of neurofibrillary tangles in P3011 tau transgenic mice induced by Abeta 42 fibrils. Science 293, 1491–1495. https://doi.org/10.1126/science.1062097 293/5534/1491 [pii], 2001/08/25.

Gouw, A.A., Seewann, A., Vrenken, H., et al., 2008. Heterogeneity of white matter hyperintensities in Alzheimer's disease: post-mortem quantitative MRI and neuropathology. Brain 131, 3286–3298. https://doi.org/10.1093/brain/awn265 awn265 [pii], 2008/10/18.

Grandjean, J., Derungs, R., Kulic, L., et al., 2016. Complex interplay between brain function and structure during cerebral amyloidosis in APP transgenic mouse strains revealed by multi-parametric MRI comparison. Neuroimage 134, 1–11, 2016/04/02. DOI: S1053-8119(16)00247-0 [pii] 10.1016/j.neuroimage.2016.03.042.

Guo, H., Albrecht, S., Bourdeau, M., et al., 2004. Active caspase-6 and caspase-6-cleaved tau in neuropil threads, neuritic plaques, and neurofibrillary tangles of Alzheimer's disease. Am. J. Pathol. 165, 523–531, 2004/07/28. DOI: S0002-9440(10)63317-2 [pii] 10.1016/S0002-9440(10)63317-2.

Hasan, K.M., Narayana, P.A., 2003. Computation of the fractional anisotropy and mean diffusivity maps without tensor decoding and diagonalization: theoretical analysis and validation. Magn. Reson. Med. 50, 589–598. https://doi.org/10.1002/mrm.10552, 2003/08/27.

Ho, W.L., Leung, Y., Cheng, S.S., et al., 2015. Investigating degeneration of the retina in young and aged tau P301L mice. Life Sci. 124, 16–23. https://doi.org/10.1016/j.lfs.2014.12.019 S0024-3205(15)00002-8 [pii], 2015/01/17.

Iba, M., Guo, J.L., McBride, J.D., et al., 2013. Synthetic tau fibrils mediate transmission of neurofibrillary tangles in a transgenic mouse model of Alzheimer's-like tauopathy. J. Neurosci. 33, 1024–1037. https://doi.org/10.1523/JNEUROSCI.2642-12.2013, 2013/01/18.

Iba, M., McBride, J.D., Guo, J.L., et al., 2015. Tau pathology spread in PS19 tau transgenic mice following locus coeruleus (LC) injections of synthetic tau fibrils is determined by the LC's afferent and efferent connections. Acta Neuropathol. 130, 349–362. https://doi.org/10.1007/s00401-015-1458-4, 2015/07/08.

Kanaan, N.M., Pigino, G.F., Brady, S.T., et al., 2013. Axonal degeneration in Alzheimer's disease: when signaling abnormalities meet the axonal transport system. Exp. Neurol. 246, 44–53. https://doi.org/10.1016/j.expneurol.2012.06.003 S0014-4886(12)00238-5 [pii], 2012/06/23.

Kantarci, K., Murray, M.E., Schwarz, C.G., et al., 2017. White-matter integrity on DTI and the pathologic staging of Alzheimer's disease. Neurobiol. Aging 56, 172–179, 2017/05/30. DOI: S0197-4580(17)30152-5 [pii] 10.1016/j.neurobiolaging.2017.04.024.

Kastyak-Ibrahim, M.Z., Di Curzio, D.L., Buist, R., et al., 2013. Neurofibrillary tangles and plaques are not accompanied by white matter pathology in aged triple transgenic-Alzheimer disease mice. Magn. Reson. Imaging 31, 1515–1521. https://doi.org/10.1016/j.mri.2013.06.013 S0730-725X(13)00230-0 [pii], 2013/09/03.

Kneynsberg, A., Combs, B., Christensen, K., et al., 2017. Axonal degeneration in tauopathies: disease relevance and underlying mechanisms. Front. Neurosci. 11, 572. https://doi.org/10.3389/fnins.2017.00572, 2017/11/02.

Kopeikina, K.J., Hyman, B.T., Spires-Jones, T.L., 2012. Soluble forms of tau are toxic in Alzheimer's disease. Transl. Neurosci. 3, 223–233. https://doi.org/10.2478/s13380-012-0032-y, 2012/10/03.

Kowall, N.W., Kosik, K.S., 1987. Axonal disruption and aberrant localization of tau protein characterize the neuropil pathology of Alzheimer's disease. Ann. Neurol. 22, 639–643. https://doi.org/10.1002/ana.410220514, 1987/11/01.

Lewis, J., McGowan, E., Rockwood, J., et al., 2000. Neurofibrillary tangles, amyotrophy and progressive motor disturbance in mice expressing mutant (P301L) tau protein. Nat. Genet. 25, 402–405. https://doi.org/10.1038/78078, 2000/08/10.

Liu, Y., Spulber, G., Lehtimaki, K.K., et al., 2011. Diffusion tensor imaging and tract-based spatial statistics in Alzheimer's disease and mild cognitive impairment. Neurobiol. Aging 32, 1558–1571. https://doi.org/10.1016/j.neurobiolaging.2009.10.006 S0197-4580(09)00336-4 [pii], 2009/11/17.

Ljungberg, M.C., Ali, Y.O., Zhu, J., et al., 2012. CREB-activity and nmnat2 transcription are down-regulated prior to neurodegeneration, while NMNAT2 over-expression is neuroprotective, in a mouse model of human tauopathy. Hum. Mol. Genet. 21, 251–267. https://doi.org/10.1093/hmg/ddr492.

Masliah, E., Mallory, M., Hansen, L., et al., 1993. An antibody against phosphorylated neurofilaments identifies a subset of damaged association axons in Alzheimer's disease. Am. J. Pathol. 142, 871–882, 1993/03/01.

Matsuoka, Y., Gray, A.J., Hirata-Fukae, C., et al., 2007. Intranasal NAP administration reduces accumulation of amyloid peptide and tau hyperphosphorylation in a transgenic mouse model of Alzheimer's disease at early pathological stage. J. Mol. Neurosci. 31, 165–170, 2007/05/05. DOI: JMN:31:2:165 [pii].

Matsuoka, Y., Jouroukhin, Y., Gray, A.J., et al., 2008. A neuronal microtubule-interacting agent, NAPVSIPQ, reduces tau pathology and enhances cognitive function in a mouse model of Alzheimer's disease. J. Pharmacol. Exp. Therapeut. 325, 146–153. https://doi.org/10.1124/jpet.107.130526 jpet.107.130526 [pii], 2008/01/18.

McAleese, K.E., Firbank, M., Dey, M., et al., 2015. Cortical tau load is associated with white matter hyperintensities. Acta Neuropathol Commun 3. https://doi.org/10.1186/s40478-015-0240-0 10.1186/s40478-015-0240-0 [pii], 60. 2015/10/01.

Mitew, S., Kirkcaldie, M.T., Halliday, G.M., et al., 2010. Focal demyelination in Alzheimer's disease and transgenic mouse models. Acta Neuropathol. 119, 567–577. https://doi.org/10.1007/s00401-010-0657-2, 2010/03/04.

Naismith, R.T., Xu, J., Tutlam, N.T., et al., 2009. Disability in optic neuritis correlates with diffusion tensor-derived directional diffusivities. Neurology 72, 589–594. https://doi.org/10.1212/01.wnl.0000335766.22758.cd 01.wnl.0000335766.22758.cd [pii], 2008/12/17.

Nikolaev, A., McLaughlin, T., O'Leary, D.D., et al., 2009. APP binds DR6 to trigger axon pruning and neuron death via distinct caspases. Nature 457, 981–989. https://doi.org/10.1038/nature07767 nature07767 [pii], 2009/02/20.

Nir, T.M., Jahanshad, N., Villalon-Reina, J.E., et al., 2013. Effectiveness of regional DTI measures in distinguishing Alzheimer's disease, MCI, and normal aging. Neuroimage-Clin 3, 180–195. https://doi.org/10.1016/j.nicl.2013.07.006.

Nishioka, C., Poh, C., Sun, S.W., 2015. Diffusion tensor imaging reveals visual pathway damage in patients with mild cognitive impairment and Alzheimer's disease. J Alzheimers Dis 45, 97–107. https://doi.org/10.3233/JAD-141239 N385Q6518524Q2N2 [pii], 2014/12/30.

Peeraer, E., Bottelbergs, A., Van Kolen, K., et al., 2015. Intracerebral injection of preformed synthetic tau fibrils initiates widespread tauopathy and neuronal loss in the brains of tau transgenic mice. Neurobiol. Dis. 73, 83–95. https://doi.org/10.1016/j.nbd.2014.08.032, 2014/09/16.

Pooler, A.M., Polydoro, M., Maury, E.A., et al., 2015. Amyloid accelerates tau propagation and toxicity in a model of early Alzheimer's disease. Acta Neuropathol Commun 3. https://doi.org/10.1186/s40478-015-0199-x s40478-015-0199-x [pii], 14. 2015/04/09.

Sahara, N., Perez, P.D., Lin, W.L., et al., 2014. Age-related decline in white matter integrity in a mouse model of tauopathy: an in vivo diffusion tensor magnetic resonance imaging study. Neurobiol. Aging 35, 1364–1374. https://doi.org/10.1016/j.neurobiolaging.2013.12.009 S0197-4580(13)00648-9 [pii], 2014/01/15.

Scheltens, P., Barkhof, F., Leys, D., et al., 1995. Histopathologic correlates of white matter changes on MRI in Alzheimer's disease and normal aging. Neurology 45, 883–888, 1995/05/01.

Schmierer, K., Wheeler-Kingshott, C.A., Boulby, P.A., et al., 2007. Diffusion tensor imaging of post mortem multiple sclerosis brain. Neuroimage 35, 467–477, 2007/01/30. DOI: S1053-8119(06)01198-0 [pii] 10.1016/j.neuroimage.2006.12.010.

Schmierer, K., Wheeler-Kingshott, C.A., Tozer, D.J., et al., 2008. Quantitative magnetic resonance of postmortem multiple sclerosis brain before and after fixation. Magn. Reson. Med. 59, 268–277. https://doi.org/10.1002/mrm.21487, 2008/01/30.

Selenica, M.L., Brownlow, M., Jimenez, J.P., et al., 2013. Amyloid oligomers exacerbate tau pathology in a mouse model of tauopathy. Neurodegener. Dis. 11, 165–181. https://doi.org/10.1159/000337230 000337230 [pii], 2012/07/17.

Sexton, C.E., Kalu, U.G., Filippini, N., et al., 2011. A meta-analysis of diffusion tensor imaging in mild cognitive impairment and Alzheimer's disease. Neurobiol. Aging 32, 2322 e2325–2318. https://doi.org/10.1016/j.neurobiolaging.2010.05.019 S0197-4580(10)00233-2 [pii], 2010/07/14.

Shin, R.W., Iwaki, T., Kitamoto, T., et al., 1992. Massive accumulation of modified tau and severe depletion of normal tau characterize the cerebral cortex and white matter of Alzheimer's disease. Demonstration using the hydrated autoclaving method. Am. J. Pathol. 140, 937–945, 1992/04/01.

Shu, X., Qin, Y.Y., Zhang, S., et al., 2013. Voxel-based diffusion tensor imaging of an APP/PS1 mouse model of Alzheimer's disease. Mol. Neurobiol. 48, 78–83. https://doi.org/10.1007/s12035-013-8418-6, 2013/07/24.

Singh, S., Dallenga, T., Winkler, A., et al., 2017. Relationship of acute axonal damage, Wallerian degeneration, and clinical disability in multiple sclerosis. J. Neuroinflammation 14. https://doi.org/10.1186/s12974-017-0831-8 10.1186/s12974-017-0831-8 [pii], 57. 2017/03/18.

Soares, J.M., Marques, P., Alves, V., et al., 2013. A hitchhiker's guide to diffusion tensor imaging. Front. Neurosci. 7 https://doi.org/10.3389/fnins.2013.00031, 31. 2013/03/15.

Song, S.K., Sun, S.W., Ramsbottom, M.J., et al., 2002. Dysmyelination revealed through MRI as increased radial (but unchanged axial) diffusion of water. Neuroimage 17, 1429–1436, 2002/11/05. DOI: S105381190291267X [pii].

Song, S.K., Kim, J.H., Lin, S.J., et al., 2004. Diffusion tensor imaging detects age-dependent white matter changes in a transgenic mouse model with amyloid deposition. Neurobiol. Dis. 15, 640–647. https://doi.org/10.1016/j.nbd.2003.12.003 S0969996103002687 [pii], 2004/04/02.

Stancu, I.C., Vasconcelos, B., Ris, L., et al., 2015. Templated misfolding of Tau by prion-like seeding along neuronal connections impairs neuronal network function and associated behavioral outcomes in Tau transgenic mice. Acta Neuropathol. 129, 875–894. https://doi.org/10.1007/s00401-015-1413-4, 2015/04/12.

Sun, S.W., Song, S.K., Harms, M.P., et al., 2005. Detection of age-dependent brain injury in a mouse model of brain amyloidosis associated with Alzheimer's disease using magnetic resonance diffusion tensor imaging. Exp. Neurol. 191, 77–85, 2004/12/14. DOI: S0014-4886(04)00374-7 [pii] 10.1016/j.expneurol.2004.09.006.

Sun, S.W., Nishioka, C., Labib, W., et al., 2015. Axonal terminals exposed to amyloid-beta may not lead to pre-synaptic axonal damage. J Alzheimers Dis 45, 1139–1148. https://doi.org/10.3233/JAD-142154 UKKQN2V730N76V05 [pii], 2015/02/24.

Sun, S.W., Nishioka, C., Chung, C.F., et al., 2017. Anterograde-propagation of axonal degeneration in the visual system of wlds mice characterized by diffusion tensor imaging. J. Magn. Reson. Imag. 45, 482–491. https://doi.org/10.1002/jmri.25368, 2016/07/05.

Umahara, T., Tsuchiya, K., Ikeda, K., et al., 2002. Demonstration and distribution of tau-positive glial coiled body-like structures in white matter and white matter threads in early onset Alzheimer's disease. Neuropathology 22, 9–12, 2002/05/28.

Uribe, V., Wong, B.K., Graham, R.K., et al., 2012. Rescue from excitotoxicity and axonal degeneration accompanied by age-dependent behavioral and neuroanatomical alterations in caspase-6-deficient mice. Hum. Mol. Genet. 21, 1954–1967. https://doi.org/10.1093/hmg/dds005 dds005 [pii], 2012/01/21.

van der Walt, A., Kolbe, S.C., Wang, Y.E., et al., 2013. Optic nerve diffusion tensor imaging after acute optic neuritis predicts axonal and visual outcomes. PLoS One 8. https://doi.org/10.1371/journal.pone.0083825 PONE-D-13-29907 [pii] e83825. 2014/01/05.

Vana, L., Kanaan, N.M., Ugwu, I.C., et al., 2011. Progression of tau pathology in cholinergic Basal forebrain neurons in mild cognitive impairment and Alzheimer's disease. Am. J. Pathol. 179, 2533–2550. https://doi.org/10.1016/j.ajpath.2011.07.044 S0002-9440(11)00766-8 [pii], 2011/09/29.

Wells, J.A., O'Callaghan, J.M., Holmes, H.E., et al., 2015. In vivo imaging of tau pathology using multi-parametric quantitative MRI. Neuroimage 111, 369–378. https://doi.org/10.1016/j.neuroimage.2015.02.023 S1053-8119(15)00124-X [pii], 2015/02/24.

Wu, J.W., Herman, M., Liu, L., et al., 2013. Small misfolded Tau species are internalized via bulk endocytosis and anterogradely and retrogradely transported in neurons. J. Biol. Chem. 288, 1856–1870. https://doi.org/10.1074/jbc.M112.394528, 2012/11/29.

Yoshita, M., Fletcher, E., Harvey, D., et al., 2006. Extent and distribution of white matter hyperintensities in normal aging, MCI, and AD. Neurology 67, 2192–2198, 2006/12/28. DOI: 67/12/2192 [pii] 10.1212/01.wnl.0000249119.95747.1f.

Zago, W., Buttini, M., Comery, T.A., et al., 2012. Neutralization of soluble, synaptotoxic amyloid beta species by antibodies is epitope specific. J. Neurosci. 32, 2696–2702. https://doi.org/10.1523/JNEUROSCI.1676-11.2012 32/8/2696 [pii], 2012/02/24.

Zerbi, V., Kleinnijenhuis, M., Fang, X., et al., 2013. Gray and white matter degeneration revealed by diffusion in an Alzheimer mouse model. Neurobiol. Aging 34, 1440–1450. https://doi.org/10.1016/j.neurobiolaging.2012.11.017 S0197-4580(12)00594-5 [pii], 2013/01/01.

Zhang, B., Carroll, J., Trojanowski, J.Q., et al., 2012. The microtubule-stabilizing agent, epothilone D, reduces axonal dysfunction, neurotoxicity, cognitive deficits, and Alzheimer-like pathology in an interventional study with aged tau transgenic mice. J. Neurosci. 32, 3601–3611. https://doi.org/10.1523/JNEUROSCI.4922-11.2012 32/11/3601 [pii], 2012/03/17.